

# MODEL BASED SYMMETRIC INFORMATION THEORETIC LARGE DEFORMATION MULTI-MODAL IMAGE REGISTRATION

*Peter Lorenzen, Brad Davis, and Sarang Joshi*

University of North Carolina, Chapel Hill  
(lorenzen,davisb,joshi)@cs.unc.edu

## ABSTRACT

This paper presents a Bayesian framework for generating inverse-consistent inter-subject large deformation transformations between two multi-modal image sets of the brain. In this framework, the estimated transformations are generated using the maximal information about the underlying neuroanatomy present in each of the different modalities. This modality independent registration framework is achieved using the Bayesian paradigm and jointly estimating the posterior densities associated with the multi-modal image sets and the high-dimensional registration transformation mapping the two subjects. To maximally use the information present in all the modalities, Kullback-Leibler divergence between the estimated posteriors is minimized to estimate the registration. Registration results for two synthetic image sets of a human neuroanatomy are presented.

*Key Words:* Multi-modal image registration, inverse consistent registration, information theory, medical image analysis, computational anatomy.

## 1. INTRODUCTION

With the increasing number of imaging techniques and imaging sensors, multi-modal image registration has become an active area of research in medical image analysis. Additionally, understanding anatomical variability requires robust high-dimensional image registration methods. Most image registration algorithms find a mapping between two scalar images. If the images are of different modalities, mutual information is typically used to register them. High-dimensional image registration in the context of mutual information and other dissimilarity measures frameworks has been studied extensively. A thorough investigation of these dissimilarity measures in high-dimensional image registration is presented in [1]. Although inter-subject high-dimensional image registration has received much attention [2, 3, 4, 5], to our knowledge, little attention has been given to using multi-modal image sets of subjects to estimate registration transformations. The extension of mutual information to three or more images is not clear.

Mutual information methods for image registration are non-model based and hence do not incorporate a priori knowledge of a subject's underlying anatomy being imaged. We incorporate anatomical structures as a prior in a Bayesian framework. As described in [6] we assume that the underlying neuroanatomy, represented in two acquired sets of multi-modal images, consists of  $N$  separate structures (or classes),  $c_i, i = 1, \dots, N$ . Let subject "1" be characterized by  $m$  multi-modal images so that  $\bar{I}_1(y) \in \mathbb{R}^m$  and subject "2" be characterized by  $n$  multi-modal images  $\bar{I}_2(z) \in \mathbb{R}^n$ , where  $c_i(\cdot)$  is the class associated with spatial positions  $y = [y_1, y_2, y_3]^T \in \Omega_1$  and  $z = [z_1, z_2, z_3]^T \in \Omega_2$  respectively. For example,  $\bar{I}_1(y)$  might represent a CT image, an T1-weighted MR image, and a PET image of a single anatomy. Throughout this paper, we assume that, for a given subject, the multi-modal images of that subject are co-registered.

### 1.1. Inverse Consistent Registration

Many registration algorithms are not inverse consistent since their dissimilarity metrics are computed in the coordinate system of either one of the images involved in the registration. This leads to order non-preservation of optimization energy cost functions. In traditional techniques for image registration solutions may be systematically biased with respect to expanding and contracting regions in the transformation [7]. Inverse consistent registration is desired when there is no preference, or believability, for one image of another. Existing methods for generating inverse consistent registration approximate inverse consistency by adding an inverse consistency penalty to the optimization cost function. The registration frameworks formulated in these methods are not intrinsically symmetric. A method for approaching this problem involving an algorithm that estimates incremental transformations while approximating inverse consistency constraints on each incremental transformation is presented in [8]. The approach presented in this paper is intrinsically inverse consistent as the registration problem is formulated symmetrically. Therefore, no correction penalty for consistency is required.

## 2. REGISTRATION FRAMEWORK

We consider the problem of finding a mapping between image sets  $\bar{I}_1$  and  $\bar{I}_2$  (Figure 1). That is, we would like to find the mappings  $f : \Omega_1 \rightarrow \Omega_2$  and  $g : \Omega_2 \rightarrow \Omega_1$  where  $\Omega_1$  and  $\Omega_2$  are the coordinate systems of image sets  $\bar{I}_1$  and  $\bar{I}_2$  respectively. We introduce a new coordinate system  $\Omega$ , independent of  $\Omega_1$  and  $\Omega_2$ . Let transformations  $h_1$  and  $h_2$  map  $\Omega$  to  $\Omega_1$  and  $\Omega_2$  respectively. By construction,  $f = h_2 \circ h_1^{-1}$  and  $g = h_1 \circ h_2^{-1}$ . This registration method is inverse consistent as  $f \circ g = g \circ f = Id$ , the identity map.

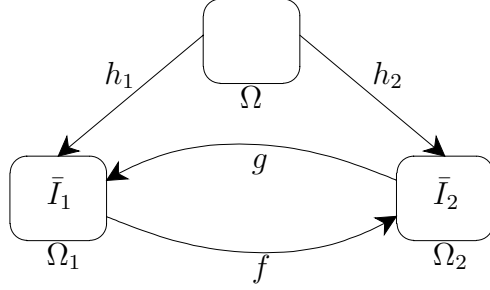


Fig. 1. Registration Framework

We apply the theory of large deformation fluid diffeomorphism of [9, 3] to require that the deformations  $h_1(x)$  and  $h_2(x)$  be solutions to the Lagrangian o.d.e.s  $\frac{d}{dt}h_{\{1,2\}}(x, t) = v_{\{1,2\}}(h_{\{1,2\}}(x, t), t)$ . The transformations  $h_1$  and  $h_2$  are generated by integrating velocity fields forward in time and  $h_1^{-1}$  and  $h_2^{-1}$  are generated by integrating velocity fields backward in time. The relationship between spatial locality, velocity fields, and time is shown in Figure 2. The spatial location  $y$  is described in terms of the forward integration of the velocity field  $v$  starting from spatial location  $x$ , that is,  $y = h(x, 1) = x + \int_0^1 v(h(x, \tau), \tau) d\tau$ . Similarly,  $x$  can be described in terms of integrating the reverse velocity field  $\tilde{v}$  starting at  $y$ , that is,  $x = \phi(y, 1) = y + \int_0^1 \tilde{v}(\phi(y, \tau), \tau) d\tau$ . From this figure we note that  $v(h(x, t), t) = -\tilde{v}(\phi(y, 1 - t), 1 - t)$  and, hence,  $\|Lv(x, t)\|^2 = \|L\tilde{v}(y, 1 - t)\|^2$  where  $L = \alpha \nabla^2 + \beta \nabla \cdot \nabla + \gamma$  is the Navier-Stokes operator.

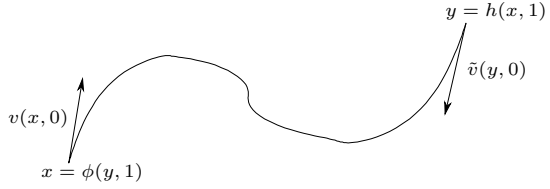


Fig. 2. Velocity Field

Given a distance metric,  $D$ , and a regularization operator  $L$ , the optimal transformations for  $h_1$  and  $h_2$  are found by estimating the velocity fields  $v_1$  and  $v_2$  following the minimization

$$\begin{aligned} \hat{v}_1, \hat{v}_2 &= \operatorname{argmin}_{v_1, v_2} \int_{\Omega} D(\bar{I}_1(h_1(x)), \bar{I}_2(h_2(x))) dx \\ &+ \int_0^1 \int_{\Omega} \|Lv_1(x)\|^2 dx dt \\ &+ \int_0^1 \int_{\Omega} \|Lv_2(x)\|^2 dx dt \end{aligned} \quad (1)$$

where  $h_{\{1,2\}}(x) = x + \int_0^1 v_{\{1,2\}}(h_{\{1,2\}}(x, t), t) dt$ . The second and third terms are the fluid regularization whose combination is symmetric by the preceding argument. For the traditional single modality mapping problem a squared error dissimilarity metric is used as described in [10].

### 2.1. Bayesian Framework

The framework is based on the assumption that human brain anatomy consists of finitely enumerable structures such as grey matter (GM), white matter (WM), and cerebrospinal fluid (CSF). These structures present with varying radiometric intensity values across disparate image modalities. Given multi-modal image sets representing two studies, we

jointly estimate, for each subject, the posterior distributions associated with each of the structures along with the diffeomorphic high-dimensional registration map that relates the coordinate spaces of the two subjects. The Kullback-Leibler divergence is used as a metric for the posterior densities to estimate the transformation. The use of the posterior probability densities provides an image intensity independent approach to image registration.

From the multi-modal images  $\bar{I}_1$  and  $\bar{I}_2$ , for each class  $c_i$  we jointly estimate the posterior distributions  $p^1(x) = p(c_i(h_1(x))|\bar{I}_1)$  and  $p^2(x) = p(c_i(h_2(x))|\bar{I}_2)$  along with the registration maps  $h_1(x)$  and  $h_2(x)$ , that map the independent coordinate space  $\Omega \subset \mathbb{R}^3$ , into the space of subject “1”,  $\Omega_1 \subset \mathbb{R}^3$ , and subject “2”,  $\Omega_2 \subset \mathbb{R}^3$ , respectively. This method is independent of the choice of the number of images comprising each image set. Optimal inter-subject multi-modal image registration is estimated by an alternating iterative algorithm which is motivated by an expectation maximization method used in [11, 12]. Our algorithm interleaves the estimation of the posteriors associated with subjects “1” and “2” and the estimation of the registration maps  $h_1 : \Omega \rightarrow \Omega_1$  and  $h_2 : \Omega \rightarrow \Omega_2$ .

Following [12], for each class  $c_i$  the associate data likelihood,  $p(\bar{I}_{\{1,2\}}(x)|c_i(x), \mu_i, \Sigma_i)$ , is modeled as a normal distribution with mean,  $\mu_i$ , and covariance,  $\Sigma_i$ . Given the transformations  $h_1$  and  $h_2$  and the current estimates  $\mu_i$  and  $\Sigma_i$  for both image sets, the posterior densities of the two subjects “1” and “2” are associated with the independent coordinate pdf  $p_i^\Omega$  by using Bayes’s Rule with  $p_i^\Omega$  as the prior for both posteriors  $p^1(x)$  and  $p^2(x)$ . Having defined the posteriors, the parameters  $\mu_i$  and  $\Sigma_i$  are updated by their expected values. We are currently investigating the use parzen

windowing as a replacement for the Gaussian models as described in [13].

## 2.2. Registration

As a measure of dissimilarity between two probability density functions  $p^\Omega(x)$  and  $p^{\{1,2\}}(x)$ , the Kullback-Leibler divergence (relative entropy),

$$D_{KL}(p^\Omega(x), p^{\{1,2\}}(x)) = \sum_{i=1}^c p_i^\Omega(x) \log \frac{p_i^\Omega(x)}{p^{\{1,2\}}(x)},$$

is used. From an information theoretic viewpoint [14], this dissimilarity can be interpreted as the inefficiency of assuming that  $p^{\{1,2\}}(x)$  is true when  $p^\Omega(x)$  is true. That is, if we have a model expressed as a probability density  $p^{\{1,2\}}(x)$ , we can then measure how far an observation, also expressed as a probability density,  $p^\Omega(x)$ , deviates from  $p^{\{1,2\}}(x)$  using Kullback-Leibler divergence.

At a given point  $x \in \Omega$  the dissimilarity between image sets  $\bar{I}_1(x)$  and  $\bar{I}_2(x)$  is measured by the dissimilarity between the posterior densities modeling them,  $p^1(x)$  and  $p^2(x)$ . We thus define the following dissimilarity metric is used to drive the registration

$$D(p^1(x), p^2(x)) = \operatorname{argmin}_{p^\Omega(x)} [D_{KL}(p^\Omega(x), p^1(x)) + D_{KL}(p^\Omega(x), p^2(x))]. \quad (2)$$

From Equation 2,  $D(p^1(x), p^2(x)) = D(p^2(x), p^1(x))$ . For known transformations  $h_1$  and  $h_2$  the probability density function in the independent coordinate system,  $p^\Omega(x)$ , that minimizes the dissimilarity measure above is the normalized geometric mean

$$p_i^\Omega(x) = \frac{(p_i^1(x)p_i^2(x))^{\frac{1}{2}}}{(p_1^1(x)p_1^2(x))^{\frac{1}{2}} + (p_2^1(x)p_2^2(x))^{\frac{1}{2}}}.$$

Thus, the dissimilarity metric can be expressed wholly in terms not involving the independent coordinate system. After substituting this value for  $p^\Omega$  into Equation 2 we obtain the following dissimilarity for position  $x \in \Omega$

$$D(p^1(x), p^2(x)) = -2 \log \sum_{i=1}^c (p_i^1(h_1(x)|\bar{I}_1)p_i^2(h_2(x)|\bar{I}_2))^{\frac{1}{2}}.$$

With this result we re-write the minimization problem stated in Equation 1 as follows

$$\begin{aligned} \hat{v}_1, \hat{v}_2 &= \operatorname{argmin}_{v_1, v_2} \int_{\Omega} \log \sum_{i=1}^c (p_i^1(h_1(x)|\bar{I}_1)p_i^2(h_2(x)|\bar{I}_2))^{\frac{1}{2}} dx \\ &+ \int_0^1 \int_{\Omega} \|Lv_1(x)\|^2 dx dt \\ &+ \int_0^1 \int_{\Omega} \|Lv_2(x)\|^2 dx dt \end{aligned}$$

## 2.3. Implementation

Following Christensen's greedy algorithm for propagating templates [15], we compute the variation for  $h_1$  of the average  $D(p^1(x), p^2(x))$  term

$$\begin{aligned} \frac{\partial}{\partial h_1} \frac{1}{|\Omega|} \int_{\Omega} D(p^1(x), p^2(x)) dx &= \\ - \frac{1}{|\Omega|} \int_{\Omega} \frac{\sum_{j=1}^c \left(\frac{p_j^2(x)}{p_j^1(x)}\right)^{\frac{1}{2}} \nabla p_j^1|_{c_j(h_1(x))}}{\sum_{k=1}^c (p_k^1(x)p_k^2(x))^{\frac{1}{2}}} dx. \end{aligned}$$

In a similar manner the variation for  $h_2$  is computed. The velocity fields  $v_{\{1,2\}}$  at each iteration are updated by solving the p.d.es.,

$$Lv_{\{1,2\}}(x, t) = \frac{\partial}{\partial h_{\{1,2\}}} \frac{1}{|\Omega|} \int_{\Omega} D(p^1(x), p^2(x)) dx.$$

The forward and backward integration is described as follows. At time  $t$  the transformations  $h_{\{1,2\}}$  are described as

$$\begin{aligned} h_{\{1,2\}}(x, t + \delta) &= h_{\{1,2\}}(x, t) + \int_t^{t+\delta} v_{\{1,2\}}(h_{\{1,2\}}(x, \tau), \tau) d\tau \\ &\approx h_{\{1,2\}}(x, t) + \delta v_{\{1,2\}}(h_{\{1,2\}}(x, t), t) \end{aligned}$$

for small  $\delta$ . At iteration  $k$  of the algorithm, the transformations  $h_{\{1,2\}}$  become the telescoping compositions  $h_{\{1,2\}} = h_{\{1,2\}}^1 \circ h_{\{1,2\}}^2 \circ \dots \circ h_{\{1,2\}}^k$ . At time  $t$  the inverse transformations  $h_{\{1,2\}}^{-1}$  are described as

$$\begin{aligned} h_{\{1,2\}}^{-1}(y, t) &= h_{\{1,2\}}^{-1}(y - \int_t^{t-\delta} v_{\{1,2\}}(y, \tau) d\tau, t - \delta) \\ &\approx h_{\{1,2\}}^{-1}(y - \delta v_{\{1,2\}}(y, t), t - \delta) \end{aligned}$$

for small  $\delta$ . At iteration  $k$  of the algorithm, the transformations  $h_{\{1,2\}}^{-1}$  become the telescoping compositions  $h_{\{1,2\}}^{-1} = h_{\{1,2\}}^{-1,k} \circ h_{\{1,2\}}^{-1,k-1} \circ \dots \circ h_{\{1,2\}}^{-1,1}$ .

## 3. RESULTS

To evaluate the performance of this algorithm we constructed two synthetic image sets comprised of images from four modalities produced by Montreal Neurological Institute's McConnell Brain Imaging Centre's BrainWeb simulated brain database [16, 17],  $\bar{I}_1 = \{\text{Proton Density, T1-weighted (Spoiled FLASH) MR}\}$  and  $\bar{I}_2 = \{\text{T1-weighted (spin echo) MR, T2-weighted MR}\}$ . The second image set,  $\bar{I}_2$  was subjected to an artificial sinusoidal transformation (Figure 3).

In order to evaluate the inverse consistency property the algorithm was applied with image sets  $\bar{I}_1$  and  $\bar{I}_2$  producing transformations  $f : \Omega_1 \rightarrow \Omega_2$  and  $g : \Omega_2 \rightarrow \Omega_1$ . The compositions  $f \circ g$  and  $g \circ f$  were then computed (Figure 4). Qualitative inspection of the regular grid under the

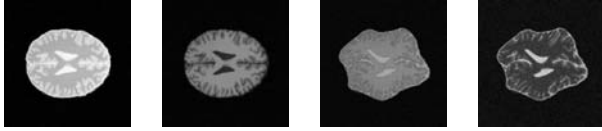


**Fig. 3.** Sample image sets: Derived from the BrainWeb simulated brain database, the two images two images on the left represent a proton-density MR image and T1-weighted MR image constituting image set  $\bar{I}_1$ . The two images on the right represent deformed versions of a fictitious image and a T2-weighted MR image constituting image set  $\bar{I}_2$ .

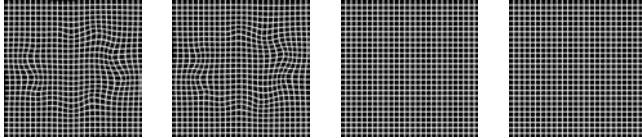


**Fig. 4.** Estimate mappings: The first two images represent a regular grid under the estimated  $f : \Omega_A \rightarrow \Omega_B$  and  $g : \Omega_B \rightarrow \Omega_A$ , transformations respectively. The last two images represent the composite transformations  $f \circ g$  and  $g \circ f$  respectively.

composite transformations  $f \circ g$  and  $g \circ f$  shows that the registration is inverse consistent. Quantitatively, the norms  $\|f \circ g - Id\|$  and  $\|g \circ f - Id\|$ , where  $Id$  represents the identity map, achieve maximums of approximately 0.2 pixels. As the original formulation is symmetric, the error can be made arbitrarily small by reducing the step size  $\delta$  in the discrete approximation. This also indicates inverse consistency. The algorithm was run for 100 iterations. The final transformed image sets are show in Figure 5.

#### 4. ACKNOWLEDGMENTS

The authors would like to thank Dr. Guido Gerig, of the department of computer science, Dr. Elizabeth Bullitt, of the department of surgery, and Marcel Prastawa of the department of computer science for their insightful suggestions and assistance during the development of this manuscript. This work was supported by NIBIB-NIH grant R01 EB000219, DOD Prostate Cancer Research Program DAMD17-03-1-0134, and the UNC-Schizophrenia Research Center, an NIMH Silvio Conte Center for the Neuroscience of Mental Disorders (MH64065).

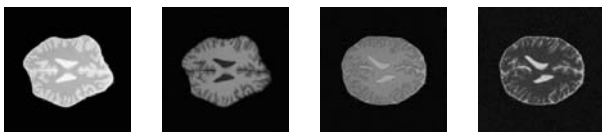


**Fig. 5.** Transformed image sets: The first two images represent the image set  $\bar{I}_1$  under the estimated mapping  $f$  and the last two images represent the image set  $\bar{I}_2$  under the mapping  $g$ .

#### 5. REFERENCES

- [1] Gerardo Valadez, *Variational Methods for Multimodal Image Matching*, Ph.D. thesis, Universite de Nice - Sophia Antipolis, May 2002.
- [2] D. Rueckert, C. Hayes, C. Studholme, P. Summers, M. Leach, and D. J. Hawkes, "Non-rigid registration of breast mr images using mutual information," *Proceedings of Medical Image Computing and Computer-Assisted Intervention*, pp. 1144–1152, 1998.
- [3] Michael Miller, Sarang Joshi, and Gary Christensen, "Large deformation fluid diffeomorphisms for landmark and image matching," in *Brain Warping*, pp. 115–131. Wiley-Interscience, 1999.
- [4] Tom Gaens, Frederik Maes, Dirk Vandermeulen, and Paul Suetens, "Non-rigid multimodal image registration using mutual information," *Proceedings of Medical Image Computing and Computer-Assisted Intervention*, pp. 1099–1106, 1998.
- [5] C. Studholme, D. L. G. Hill, and D. J. Hawkes, "An overlap invariant entropy measure of 3d medical image alignment," *Pattern Recognition*, pp. 71–86, December 1998.
- [6] Peter Lorenzen and Sarang Joshi, "High-dimensional multi-modal image registration," *Workshop on Biomedical Image Registration (WBIR)*, vol. LNCS-2717, pp. 234–243, 2003.
- [7] Pascal Cachier and David Rey, "Symmetrization of the non-rigid registration problem using inversion-invariant energies: Application to multiple sclerosis," *Medical Image Computing and Computer-Assisted Intervention (MICCAI)*, 2002.
- [8] Jianchun He and Gary Christensen, "Large deformation inverse consistent elastic registration," *Information Processing in Medical Imaging*, vol. LNCS-2732, pp. 438–449, 2003.
- [9] S. Joshi and M. I. Miller, "Landmark matching via large deformation diffeomorphisms," *IEEE Transactions on Image Processing*, vol. 9, no. 8, pp. 1357–1370, August 2000.
- [10] Brad Davis, Peter Lorenzen, and Sarang Joshi, "Large deformation minimum mean squared error template estimation for computation anatomy," *submitted to IEEE International Symposium on Biomedical Imaging (ISBI)*, 2004.
- [11] Nathan Moon, E Bullitt, K van Leemput, and Guido Gerig, "Automatic brain and tumor segmentation," *Medical Image Computing and Computer-Assisted Intervention (MICCAI)*, vol. LNCS-2489, pp. 372–379, 00–00 September 2002.
- [12] K. v. Leemput, F. Maes, D. Vandermeulen, and P. Suetens, "Automated model-based tissue classification of mr images of the brain," *IEEE Transactions on Medical Imaging (TMI)*, vol. 18, pp. 897–908, 1999.
- [13] Marcel Prastawa, Elizabeth Bullitt, Sean Ho, and Guido Gerig, "Robust estimation for brain tumor segmentation," *Medical Image Computing and Computer-Assisted Intervention (MICCAI)*, 2003.
- [14] Thomas M. Cover and Joy A. Thomas, *Elements of Information Theory*, Wiley-Interscience, New York, 1991.
- [15] G. E. Christensen, R. D. Rabbitt, and M. I. Miller, "Deformable templates using large deformation kinematics," *IEEE Transactions on Image Processing*, vol. 5, no. 10, pp. 1435–1447, October 1996.
- [16] C Cocosco, V Kollokian, R Kwan, and A Evans, "Brainweb: Online interface to a 3d mri simulate brain database," *Proceedings of the 3rd International Conference on Functional Mapping of the Human Brain*, vol. 5, no. 4, May 1997.
- [17] "<http://www.bic.mni.mcgill.ca/brainweb/>."